Electron-impact vibrational excitation of tetrahydrofuran

M. A. Khakoo, D. Orton, L. R. Hargreaves, and N. Meyer

Phys. Rev. A **88**, 012705 — Published 12 July 2013

DOI: 10.1103/PhysRevA.88.012705

Electron Impact Vibrational Excitation of Tetrahydrofuran

M. A. Khakoo[1], D. Orton[1] and L. Hargreaves[1]

[1] Department of Physics, California State University Fullerton, Fullerton, CA 92831

N. Meyer [2]

[2] Troy High School, Dorothy Lane, Fullerton, CA 92831

Abstract: Low-energy differential and integral cross-sections for the electron impact vibrational excitation of tetrahydrofuran are presented. The data concerns four features in the vibrational excitation electron energy loss spectrum of tetrahydrofuran over the energy loss range of 0 to 0.9eV. The results show weak influence from long-range dipole interactions, being mainly isotropic. Comparison with earlier work is presented.

PACS numbers: 34.80.Bm

1. Introduction.

The pioneering work by Sanche and coworkers [1, 2], which demonstrated that low-energy electrons can induce DNA strand breaks, has since drawn considerable effort to bear on low energy electron collision processes involving DNA constituents. Much of this work, both experimental and theoretical [3], has centered on tetrahydrofuran (THF), the simplest model of the furanose ring that links the phosphate groups in the DNA backbone. These studies have provided valuable information about processes relevant to understanding electron transport and reactivity in biological media including: vibrational and electronic excitation; electron trapping and reactivity in condensed THF; and elastic and total scattering cross sections. This work concerns vibrational excitation of THF.

The first electron spectroscopy study of the vibrational excitation of THF was undertaken by Lepage *et al*. [4] in the gaseous phase and solid state phase on a Pt(111) monocrystal for different THF thicknesses (up to 16 layers). They concentrated on resonant enhancement of vibrational excitation and claim to have observed the presence of 3 resonances (in the solid state) located at 4, 7.5 and 10eV, with the possibility of further overlapping higher lying resonances. For gaseous THF they observed enhancement of the v_2 mode around 8.4eV (shifted down to 7.4eV in the solid state) and assign this to the $^1n_0 3s$ highest occupied molecular orbital, viz. excitation of a 2p non-bonding electron from the oxygen heteroatom into the next higher 3s orbital, i.e. (n_0)-1 $\rightarrow$3s. They also summarize optical (IR) vibrational spectroscopy of THF from past work, most recent being Cadioli *et al*. [5]. More recently, Dampc *et al*. [6] investigated the electron impact vibrational excitation of THF in the incident electron range of 4.5 to 14 eV and for scattering angles (θ) from 20^o to 180^o, using a magnetic angle changer (MAC, see [7] for details). They identified three vibrational energy loss features, which were

ascribed approximately to predominantly C-C stretch, CH_2 collective (twist, rock) and CH_2 stretch modes at around 100meV, 140meV and 350meV energy loss values. They focused on the best resolved of these 3 features, i.e. the predominantly CH stretch modes feature at 350meV and measured its differential cross-section at E_0 values of 7 and 10eV and its excitation function at $\theta=80^o$ over an incident energy range of 4eV to14eV. In their excitation function they observed a shoulder at E_0=6eV, and a resonance maximum at E_0=7.9eV and 10.3eV. They compared their 7.9eV peak to the 8.4eV peak observed by Lepage *et al*. [4] in the gaseous phase. They also reported higher energy loss features observed at 690meV and 950meV due to higher overtones of stretch and combination modes of CH_2. Soon after, Allan [8] measured absolute angle-differential elastic and inelastic vibrational excitation cross-sections for the CC stretch modes at 114meV and 134meV energy losses, CH_2 scissoring (bending) mode at 180meV energy loss, the CH_2 stretch mode at 363meV energy loss, and overtones of the CC stretch and CH stretch modes at 228meV and 720meV. They measured differential cross-sections as a function of E_0, ranging from threshold to 16eV for these excitations for scattering angles (θ) of 135^o. For all these features, they observe broad resonant behavior with peaks at 6.2eV and 10.8eV. The 6.2eV resonance had been observed in dissociative electron attachment (negative ion formation) studies by Aflatooni *et al*. [9] who assigned it to a core-excited shape resonance, but did not give its symmetry. Allen also observed resonant enhancement of the 180meV CH_2 scissoring (bending) mode, which was interpreted by them as one similar to that observed in earlier work on cyclopropane (see discussion in [8]) and an indication of a low-lying $^2A_2$ shape resonance. Allen also gave integrated vibrational excitation cross-sections for THF at E_0 values of 6eV and 10eV.

In this work, we present absolute differential and integral cross-sections (DCS & ICS, respectively) measurements for vibrational excitation of THF for the spectral features observed in [6], i.e. spanning the intervals of 0.084 - 0.261eV, 0.262 - 0.444eV, 0.445 - 0.616eV, 0.617 - 0.796eV. The DCS were determined at E_0 values of 2eV, 3eV, 5eV, 10eV and 15eV and for θ spanning 15^o to 130^o. The DCSs were normalized to elastic DCSs taken earlier by our group [10] using an aperture-source relative flow method with He.

2. Experimental.

The experimental apparatus has been described in previous articles, e.g., Khakoo *et al*. [11]. The apparatus comprises an electron gun producing a collimated electron beam of known energy, intersecting a gas jet formed by the effusive flow of gas through a 1mm aperture to collimate the gas, and a scattered electron detector which registered and energy analyzed electrons scattered by the gas jet.

The electron gun employed titanium double hemispherical energy selectors. Typical electron currents at the collision region were around 30nA, with an energy resolution of approximately 60meV, full width at half-maximum. The electron gun (and analyzer) was baked to about 130^oC with magnetically free biaxial heaters (ARi Industries model BXX06B41-4K). Electrons scattered by the gas jet were measured by a hemispherical energy analyzer, whose design essentially mirrors the electron gun. The analyzer's detector was a discrete dynode electron multiplier (Equipe Thermodynamique et Plasmas model AF151) with a background rate of <0.01 Hz and a maximum count rate of 1MHz before saturating.

The effusive gas beam target was formed by flowing THF gas through a thin aperture source 0.3 mm in diameter described previously [13]. This source was covered with

carbon soot, using a pure acetylene flame, to reduce secondary electrons and placed 6 mm below the axis of the electron beam, incorporated into a movable source arrangement [14]. The vapor pressure behind the source for furan was about 0.3– 0.4Torr the pressure in the experimental chamber of ~$4x10^{-7}$Torr. The gas temperature in the collision region was about 130^{o}C. THF vapor was obtained from a research grade liquid THF (>99.5% purity), degassed using multiple freeze-pump-thaw cycles.

Energy loss spectra of THF were collected at fixed E_0 values and θ by repetitive multichannel-scaling techniques. The energy loss range covered was from -0.25eV to 1.25eV energy loss which covered the elastic peak and the major vibrational excitations of THF. A typical electron energy loss spectrum (EELS) is shown in Fig. 1. The assignment of the features observed in our EELS was taken from the work of LePage *et al*. [4] and Cadioli *et al*. [5]. Each EELS was analyzed by fitting Gaussian profiles at energy losses corresponding to each vibrational feature. The line profile of the spectrometer was determined using the width of the elastic feature from -0.150 to +0.040eV, while the energy loss (E_L) positions of the vibrational features were taken as assigned in [4, 5]. The spectral features could be separated into four distinct regions (see Table 1). Differential cross-sections for these regions were determined by normalizing the spectral intensities of each feature to the elastic peak line intensity using elastic differential cross-sections for THF measured earlier by our group [3]. No correction for transmission was made as the E_0 value of the spectra exceeded the E_L value of the features by a factor of 10 in most cases, in which case the transmission can reasonably be assumed to be constant.

3. Results and Discussion.

Differential cross-sections for excitation of the four energy loss features are given in Table 2, and plotted in Figure 2, along with the integral cross-sections (σ_i) and momentum transfer cross-sections (σ_m). The error bars include statistical uncertainties (<1%), uncertainty in the elastic DCS of [3], contamination of the elastic peak by vibrational excitation (±5%), and an uncertainty in the transmission of the spectrometer (±10%), summed in quadrature.

The "CC-stretch" feature (E_L=0.084 - 0.261eV) covers 6 symmetric and asymmetry stretch modes, as well as 17 other rock, wag, twist and bend/scissoring modes for CH_2 and 2 C-O-C stretch modes (listed in Table 1). These additional modes mask any dipole behavior of the CC-stretch modes. On the other hand, the "CH_2-stretch" feature (E_L=0.262 - 0.444eV) covers 6 asymmetric and symmetric CH_2 stretch modes. The next higher-lying features (E_L=0.445 - 0.616eV and 0.617 - 0.796eV) are weaker and more complicated as they contain a combination of several vibrational modes found in the ranges E_L=0.084 - 0.261eV and E_L=0.262 - 0.444eV and also a doubling up of CH-stretch modes. The latter of these two features is the weakest.

Summing all of the vibrational excitations, in Figure 2, we observe weak dipole behavior (forward scattering) between E_0=5 to 15eV with distinct forward scattering at 2 and 3 eV. At very low energy the role of the dipole is expected to be dominant, but at E_0=5eV to 15eV we observe essentially isotropic behavior, similar to that which was observed by us in a similar investigation in furan [15]. In fact at E_0=15eV we observe a fall in the DCS towards zero angle. At E_0=20eV, weak forward scattering is once again observed. This behavior for a molecule with a strong dipole moment indicates that the transition moment depends on the dynamic change of dipole moment, rather than the

influence of a static dipole, as the excitation promotes the molecule from the ground level to the vibrationally excited level, with the rotational states averaged over the vibrational excitation. However at incident energies of 2eV and 3eV, where the static dipole is very dominant, vibrational excitation is likely coupled to the elastic scattering. Consequently we attribute the distinct forward scattering to such an effect, especially at 2eV.

The "CC-stretch" (E_L=0.083 - 0.261eV) and the "CH_2-stretch" energy loss lines (E_L=0.262 - 0.444eV), being dominant features of the vibrational energy loss spectrum both show similar show forward peaking at the same E_0 values as the sum of the vibrational features. For the dominant CH_2-stretch feature we can compare, at E_0=10eV, with the recent work of Dampc *et al*. [6], who observe strong forward scattering at this E_0 value. However, forward scattering is absent in the present data, in the interval of E_0 from 5eV to 15eV. The results of Dampc *et al*. are also smaller than then than present data, by an average factor of 1.3. This factor is can be partially explained by the elastic DCSs used to normalize their data, which are higher than ours in at by 16% on average, but around 30% at $\theta \leq 30^o$. We note that a comparison of elastic scattering DCSs with the similar study of Colyer *et al*. [16], gives excellent agreement of 6% on average, and around 17% at $\theta \leq 30^o$, which is within the combined error estimates of both measurements. With the scaling, we observe very good agreement between the two measurements for vibrational excitation of the "CH_2-stretch" feature, mostly within error bars of the measurements except at their lowest θ of 20^o. We do not observe the d-wave dominance in the DCS for this feature as clearly they do, instead seeing a more isotropic type distribution.

For the two higher-lying features, the DCSs show mostly isotropic angular behavior. At E_0=3eV, the E_L=0.445 - 0.616eV feature shows a clear peak around $\theta=80^o$. The contribution of these features is a factor of ≈10 or more lower than the CH_2-stretch

feature. In some respects this is similar to what we observed for furan in a similar work [15]. At our highest E_0 value, the DCSs for these features are of the same magnitude.

In Figure 3, we plot the σ_i for the four features as well as their sum. These integral cross-sections were obtained by integrating the DCSs at all solid angles and extrapolating the measurements to 0^o and to 180^o. The extrapolation method and its inclusion in the error estimates is discussed in detail in [3]. In this case, since these DCSs are mostly isotropic in angular distribution, the additional error in extrapolating them was < 5%. All the present σ_i maximize around $E_0 \approx 8$eV. This is in the same region as the ^2B resonance (C_2 point group symmetry) observed in elastic scattering observed earlier by our group [3] and indicates the strong coupling between vibrational excitation as a result of resonant elastic scattering in the post-collision process.

4. Conclusions.

We have measure DCSs for vibrational excitation for four features in the vibrational energy loss spectrum of THF observed with moderate resolution. The DCSs show similar trends as was observed earlier by us for furan [3], primarily that they are not forward-peaked typical of dipole excitations. Since the measurements did not resolve individual vibrational modes, this work should be followed by a higher resolution study, as done by Allan [8], in an effort to investigate forward-scattering vibrational stretch modes.

5. Acknowledgements.

This work was supported by the National Science Foundation under Grants No. RUI-PHY-0965793 and PHY 0653452.

6. References.

[1] B. Boudaïffa, P. Cloutier, D. Hunting, M. A. Huels, and L. Sanche, Science **287**, 1658 (2000).

[2] M. A. Huels, B. Boudaïffa, P. Cloutier, D. Hunting, and L. Sanche, J. Am. Chem. Soc. **125**, 4467 (2003).

[3] A. Gauf, L. R. Hargreaves, A. Jo, J. Tanner, M. A. Khakoo, T. Walls, C. Winstead and V. McKoy, Phys. Rev. A **85**, 052717 (2012).

[4] Lepage, S. Letarte, M. Michaud, F. Motte-Tollet, M.-J. Hubin-Franskin, D. Roy, and L. Sanche, J. Chem. Phys. **109**, 5980 (1998).

[5] B. Cadioli, E. Gallinella, C. Coulombeau, H. Jobic and G. Berthier, J. Chem. Phys. **97**, 7844 (1993).

[6] M. Dampc, I. Linert, A. R. Milosavljević, and M. Zubek, Chem. Phys. Letts. **443**, 17 (2007).

[7] I. Linert and M. Zubek, J. Phys. B **39**, 4087 (2006).

[8] M. Allan, J. Phys. B **40**, 3531 (2007).

[9] K. Aflatooni, A. M. Scheer and P. D. Burrow, J. Chem. Phys. **125**, 054301 (2006).

[10] A. Gauf, L. R. Hargreaves, A. Jo, J. Tanner, M. A. Khakoo, T. Walls, C. Winstead and V. McKoy, Phys. Rev. A **85**, 052717 (2012).

[11] M. A. Khakoo, C. E. Beckmann, S. Trajmar, and G. Csanak, J. Phys. B **27**, 3159 (1994).

[12] J. H. Brunt, G. C. King, and F. H. Read, J. Phys. B **10**, 1289 (1977).

[13] M. A. Khakoo, H. Silva, J. Muse, M. C. A. Lopes, C. Winstead, and V. McKoy, Phys. Rev. A **78**, 052710 (2008).

[14] M. Hughes, K. E. James, Jr., J. G. Childers, and M. A. Khakoo, Meas. Sci. Technol. **14**, 841 (1994).

[15] L. R. Hargreaves, R. Albaridy, G. Serna, M. C. A. Lopes and M. A. Khakoo, Phys. Rev A. **81**, 062705 (2011).

[16] C. J. Colyer, V. Vizcaino, J. P. Sullivan, M. J. Brunger, and S. J. Buckman, New J. Phys. **9**, 41 (2007).

7. Tables.

Feature	E_L (eV)	Symmetry	I.D.	Mode Type
Elastic	0.000	A		
	0.017	B	ν_{33}	ring pucker + β-CH_2 twist
	0.037	A	ν_{17}	ring pucker
	0.073	B	ν_{32}	ring bend + β-CH_2 rock
0.084-0.261	0.083	A	ν_{16}	ring bend
	0.104	A	ν_{15}	β and α-CH_2 rock
	0.107	B	ν_{31}	β-CH_2 rock + ring bend
	0.109	A	ν_{14}	C-O-C sym. stretch
	0.113	B	ν_{30}	$C_\alpha C_\beta$ asym. stretch + β-CH_2 twist
	0.115	A	ν_{13}	$C_\beta C_\beta$ asym. stretch + $C_\alpha C_\beta$ asym. stretch
	0.119	B	ν_{29}	β-CH_2 rock + $C_\alpha C_\beta$ asym. stretch
	0.129	A	ν_{12}	β-CH_2 wag + $C_\alpha C_\beta$ sym. stretch
	0.131	B	ν_{28}	C-O-C asym. stretch
	0.142	A	ν_{11}	α-CH_2 rock + β-CH_2 rock
	0.144	B	ν_{27}	α-CH_2 twist + β-CH_2 rock
	0.147	A	ν_{10}	α-CH_2 twist + β-CH2 wag +..
	0.154	A	ν_9	α– and β-CH_2 twist
	0.155	B	ν_{26}	β– and α-CH_2 twist
	0.161	B	ν_{25}	β– and α-CH_2 wag
	0.163	A	ν_8	β–CH_2 wag and α-CH_2 wag
	0.166	B	ν_{24}	α– and β-CH_2 wag
	0.170	A	ν_7	α-CH_2 wag
	0.179	B	ν_{23}	CH_2 bend/scissoring
	0.183	A	ν_6	CH_2 bend/scissoring
	0.185	B	ν_{22}	CH_2 bend/scissoring
	0.187	A	ν_5	CH_2 bend/scissoring
	0.228	A	$2\nu_{12}$	2xCC asym./sym. stretch
0.262-0.444	0.354	B	ν_{21}	α-CH_2 sym. stretch
	0.357	A	ν_4	α-CH_2 sym. stretch
	0.362	A	ν_3	β-CH_2 sym. stretch
	0.362	B	ν_{20}	β-CH_2 sym. stretch
	0.364	B	ν_{19}	α-CH_2 asym. stretch
	0.366	A	ν_2	α-CH_2 asym. stretch
	0.369	A	ν_1	β-CH_2 asym. stretch
	0.370	B	ν_{18}	β-CH_2 asym. stretch
0.445-0.616	0.480	A	$\nu_2 + \nu_{13}$	Combination E_L
	0.497	A + B	$\nu_2 + \nu_{28}$	Combination E_L
	0.517	A + B	$\nu_2 + \nu_{26}$	Combination E_L
	0.529	A	$\nu_2 + \nu_8$	Combination E_L
	0.547	A	$\nu_2 + \nu_6$	Combination E_L
0.617-0.796	0.708	B	$2\nu_{21}$	2xCH asym/sym. Stretch

Table 1. Excitation energy loss (E_L) values for vibrational modes of THF (C_2 symmetry) taken mainly from Cadioli *et al*. [5] using IR-spectroscopy and LePage *et al.* [4] using electron spectroscopy. The mode type assignments are from [5]. The E_L range of four resolved features is listed in the first column. See text for discussion.

E_L (eV)	.084-0.261	Error	0.262-0.444	Error	0.445-0.616	Error	0.617-0.796	Error	Sum	Error
					E_0 = 2 eV					
20	0.169	0.026	0.074	0.013					0.243	0.035
30	0.092	0.014	0.033	0.006					0.125	0.017
40	0.076	0.012	0.016	0.003					0.092	0.014
50	0.072	0.010	0.021	0.003					0.093	0.012
60	0.065	0.010	0.019	0.003					0.085	0.012
70	0.068	0.010	0.020	0.003					0.088	0.012
80	0.057	0.009	0.019	0.003					0.076	0.012
90	0.070	0.011	0.027	0.005					0.097	0.014
110	0.084	0.012	0.043	0.007					0.127	0.018
130	0.092	0.015	0.036	0.007					0.129	0.021
σ_i	*1.08*	*0.166*	*0.427*	*0.074*					*1.51*	*0.22*
σ_m	*1.06*	*0.162*	*0.446*	*0.077*					*1.51*	*0.22*
					E_0 = 3 eV					
20	0.168	0.025	0.085	0.015	0.0055	0.0010			0.258	0.036
30	0.124	0.022	0.057	0.011	0.0053	0.0011			0.186	0.031
40	0.106	0.016	0.043	0.007	0.0042	0.0008			0.154	0.021
50	0.103	0.015	0.046	0.008	0.0044	0.0008			0.154	0.020
60	0.107	0.017	0.050	0.009	0.0077	0.0015			0.165	0.024
70	0.116	0.022	0.056	0.011	0.0077	0.0017			0.180	0.032
80	0.115	0.023	0.054	0.012	0.0111	0.0026			0.180	0.035
90	0.097	0.018	0.051	0.010	0.0069	0.0015			0.154	0.027
110	0.089	0.014	0.043	0.008	0.0077	0.0015			0.139	0.021
130	0.088	0.014	0.047	0.008	0.0054	0.0011			0.140	0.022
σ_i	*1.31*	*0.22*	*0.648*	*0.120*	*0.0831*	*0.0169*			*2.05*	*0.32*
σ_m	*1.21*	*0.22*	*0.616*	*0.120*	*0.0828*	*0.0169*			*1.91*	*0.30*
					E_0 = 5 eV					
15	0.329	0.053	0.172	0.031	0.016	0.003	0.0043	0.0009	0.521	0.078
20	0.239	0.044	0.121	0.024	0.019	0.004	0.0046	0.0010	0.384	0.067
30	0.235	0.039	0.118	0.022	0.022	0.004	0.0057	0.0012	0.380	0.059
40	0.271	0.041	0.139	0.024	0.025	0.005	0.0051	0.0010	0.440	0.062
50	0.280	0.040	0.143	0.024	0.024	0.004	0.0057	0.0011	0.453	0.059
60	0.246	0.043	0.129	0.025	0.020	0.004	0.0055	0.0012	0.401	0.065
70	0.247	0.038	0.130	0.023	0.023	0.004	0.0058	0.0012	0.406	0.058
80	0.260	0.050	0.134	0.028	0.025	0.006	0.0076	0.0018	0.427	0.077
90	0.248	0.038	0.128	0.022	0.024	0.005	0.0076	0.0015	0.408	0.058
110	0.266	0.039	0.136	0.023	0.027	0.005	0.0081	0.0016	0.436	0.059
130	0.267	0.039	0.135	0.024	0.027	0.004976344	0.0077	0.0012	0.437	0.064
σ_i	*3.27*	*0.53*	*1.68*	*0.31*	*0.309*	*0.062*	*0.090*	*0.014*	*5.34*	*0.81*
σ_m	*3.28*	*0.54*	*1.68*	*0.31*	*0.324*	*0.065*	*0.099*	*0.015*	*5.39*	*0.82*
					E_0 = 10 eV					
15	0.293	0.061	0.109	0.024	0.012	0.003	0.0061	0.0015	0.421	0.083
20	0.274	0.057	0.101	0.023	0.013	0.003	0.0069	0.0017	0.395	0.079
30	0.286	0.059	0.109	0.024	0.016	0.004	0.0063	0.0015	0.417	0.083
40	0.272	0.061	0.114	0.027	0.016	0.004	0.0062	0.0016	0.408	0.088
50	0.284	0.056	0.117	0.025	0.018	0.004	0.0077	0.0018	0.426	0.080
60	0.260	0.052	0.112	0.024	0.015	0.004	0.0062	0.0015	0.394	0.075
70	0.237	0.038	0.101	0.018	0.015	0.003	0.0048	0.0010	0.358	0.054
80	0.251	0.055	0.111	0.026	0.016	0.004	0.0072	0.0019	0.385	0.082
90	0.267	0.058	0.128	0.029	0.016	0.004	0.0069	0.0018	0.418	0.087
110	0.327	0.063	0.149	0.031	0.019	0.004	0.0065	0.0015	0.502	0.092
130	0.335	0.060	0.151	0.030	0.021	0.004	0.0065	0.0014	0.514	0.087
σ_i	*3.74*	*0.75*	*1.63*	*0.36*	*0.221*	*0.052*	*0.0819*	*0.0199*	*5.67*	*1.10*
σ_m	*3.98*	*0.80*	*1.75*	*0.38*	*0.238*	*0.056*	*0.0820*	*0.0199*	*6.05*	*1.17*
					E_0 = 15 eV					
15	0.174	0.030	0.062	0.012	0.0052	0.0011	0.0039	0.0009	0.245	0.040
20	0.208	0.032	0.062	0.011	0.0025	0.0005	0.0028	0.0006	0.275	0.040
30	0.211	0.039	0.076	0.015	0.0052	0.0011	0.0050	0.0011	0.298	0.052
40	0.168	0.029	0.063	0.012	0.0032	0.0007	0.0039	0.0008	0.238	0.038
50	0.165	0.031	0.062	0.013	0.0044	0.0010	0.0044	0.0010	0.235	0.043
60	0.177	0.033	0.067	0.014	0.0048	0.0010	0.0049	0.0011	0.254	0.045
70	0.160	0.023	0.059	0.010	0.0058	0.0011	0.0031	0.0006	0.228	0.030
80	0.154	0.026	0.057	0.011	0.0040	0.0008	0.0027	0.0006	0.218	0.034
90	0.164	0.024	0.058	0.010	0.0032	0.0006	0.0029	0.0006	0.228	0.030
110	0.163	0.023	0.065	0.011	0.0052	0.0010	0.0027	0.0005	0.236	0.030
130	0.216	0.040	0.082	0.017	0.0050	0.0011	0.0043	0.0010	0.307	0.054
σ_i	*2.29*	*0.39*	*0.868*	*0.160*	*0.057*	*0.012*	*0.047*	*0.010*	*3.27*	*0.51*
σ_m	*2.39*	*0.40*	*0.928*	*0.171*	*0.059*	*0.012*	*0.047*	*0.010*	*3.43*	*0.53*
					E_0 = 20 eV					
10	0.247	0.036	0.044	0.007	0.0011	0.0002	0.0014	0.0003	0.295	0.039
15	0.169	0.027	0.032	0.006	0.0008	0.0002	0.0010	0.0002	0.204	0.029
20	0.164	0.024	0.033	0.006	0.0008	0.0002	0.0013	0.0003	0.199	0.027
30	0.122	0.017	0.031	0.005	0.0012	0.0002	0.0018	0.0004	0.156	0.020
40	0.103	0.015	0.025	0.004	0.0012	0.0002	0.0018	0.0003	0.130	0.017
50	0.099	0.018	0.021	0.004	0.0011	0.0002	0.0017	0.0004	0.123	0.021
60	0.092	0.017	0.021	0.004	0.0019	0.0004	0.0015	0.0003	0.116	0.021
70	0.094	0.014	0.020	0.003	0.0011	0.0002	0.0013	0.0002	0.116	0.015
80	0.093	0.016	0.021	0.004	0.0014	0.0003	0.0014	0.0003	0.117	0.019
90	0.098	0.014	0.023	0.004	0.0018	0.0003	0.0012	0.0002	0.124	0.017
110	0.103	0.018	0.026	0.005	0.0016	0.0003	0.0017	0.0004	0.133	0.021
130	0.108	0.016	0.028	0.005	0.0019	0.0004	0.0016	0.0003	0.140	0.018
σ_i	*1.34*	*0.21*	*0.322*	*0.058*	*0.020*	*0.004*	*0.019*	*0.004*	*1.71*	*0.25*
σ_m	*1.32*	*0.21*	*0.332*	*0.060*	*0.022*	*0.004*	*0.020*	*0.004*	*1.69*	*0.25*

Table 2. Present experimental differential cross-sections for electron impact vibrational excitation of THF in units of 10^{-16}cm^2/sr.

7. Figures.

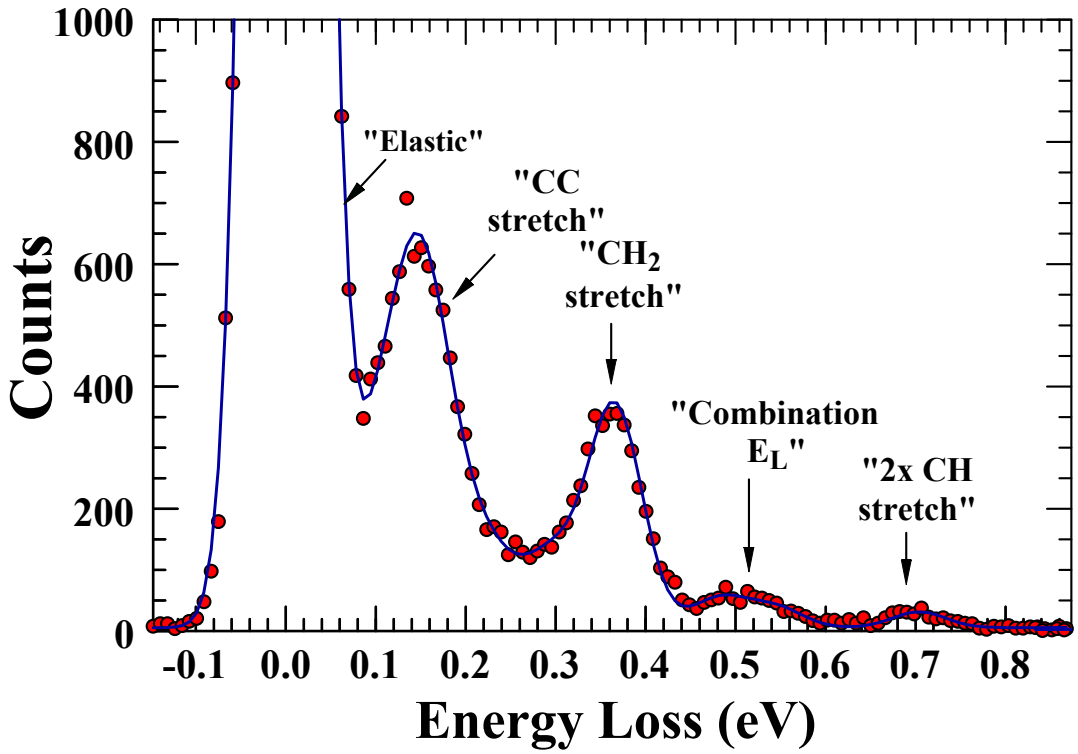

Figure 1 (Color Online): Background subtracted electron energy loss spectrum of THF at E_0=5eV and θ=60^o. The features are identified according to their most prevalent modes. See Table 1 for a listing. See text for further discussion. The line is a fit through the data points using the spectral energy loss positions of the lines in Table 1. See text for discussion.

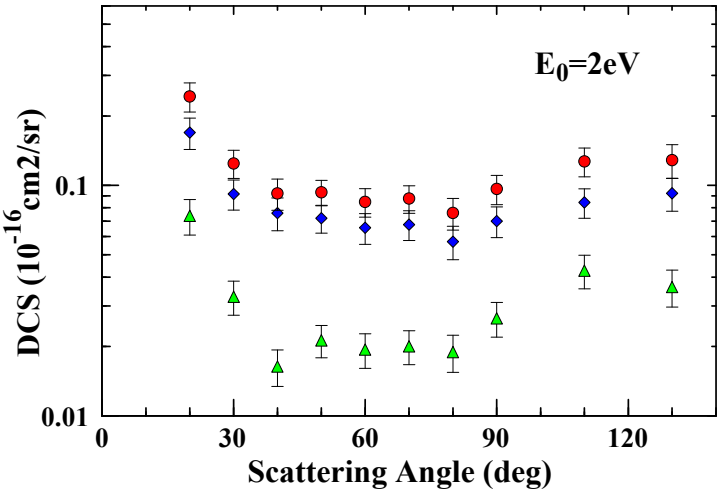
E0=2eV
DCS (10-16cm2/sr)
0.1
0.01
0
30
60
90
120
Scattering Angle (deg)

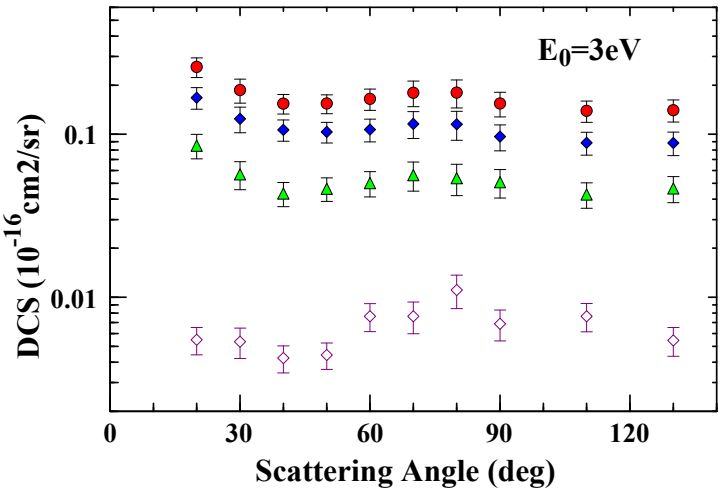
E0=3eV
DCS (10-16cm2/sr)
0.1
0.01
0
30
60
90
120
Scattering Angle (deg)

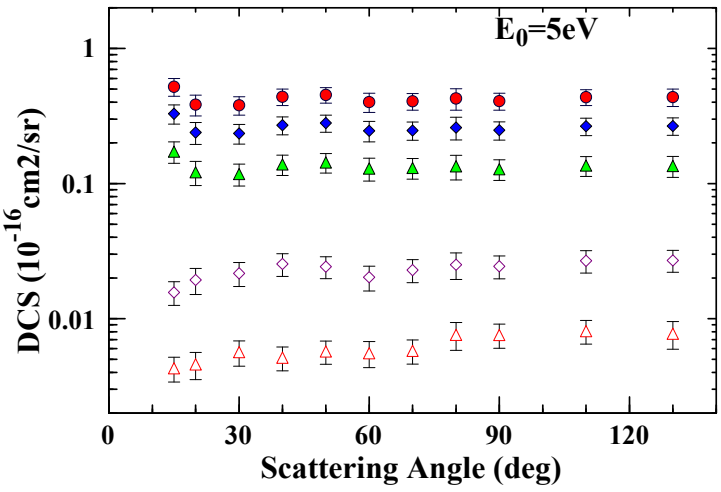
E0=5eV
DCS (10-16cm2/sr)
1
0.1
0.01
0
30
60
90
120
Scattering Angle (deg)

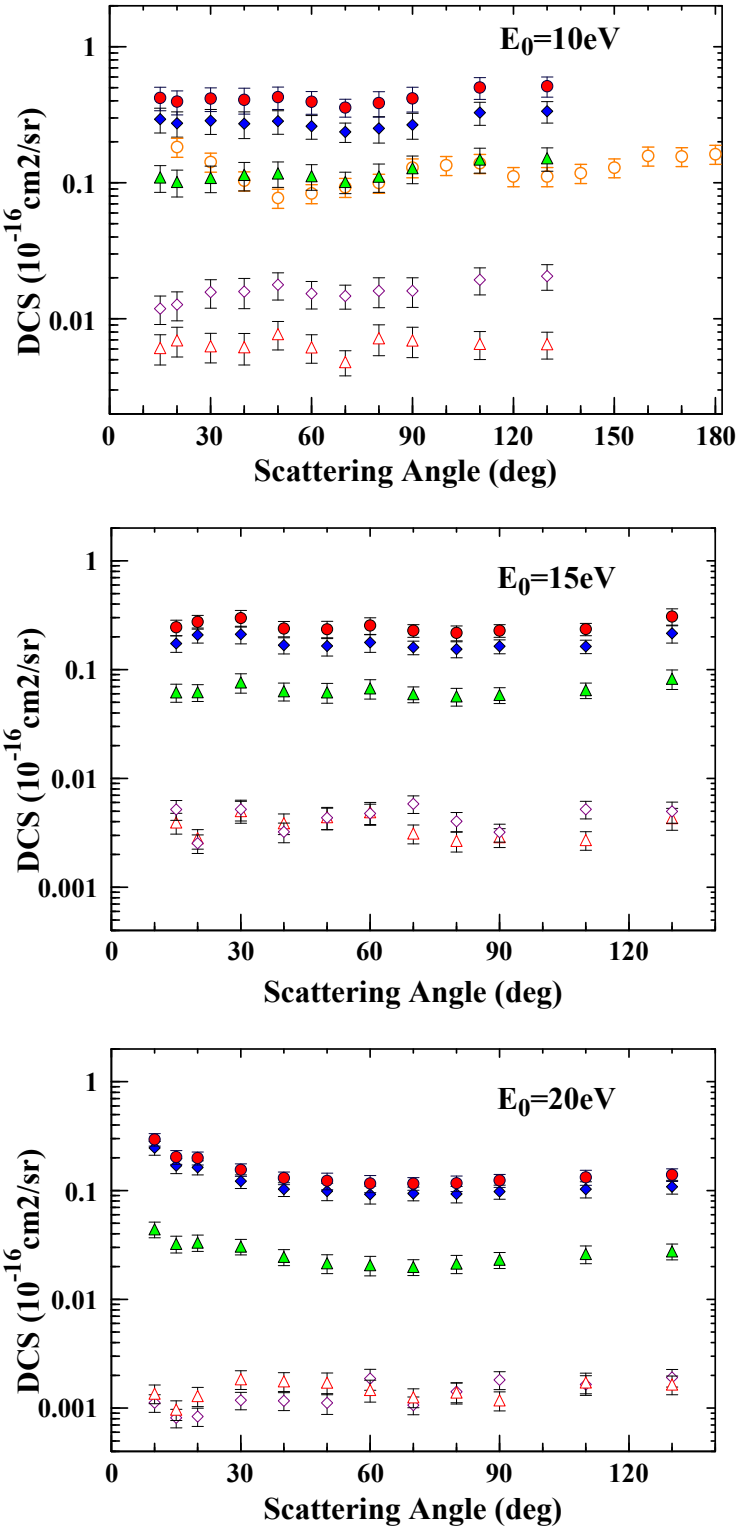

Figure 2 (Color Online): Differential cross-sections for vibrational excitation of THF at various E_0 values. Legend: ● red solid circles, total vibrational excitation from E_L=0.084 to 0.796eV; ♦ blue solid diamonds, excitation from E_L=0.084eV to 0.261eV (predominantly CC- stretch); ▲ blue solid diamonds, excitation from E_L=0.262eV to 0.444eV (mostly CH_2- stretch); ◊ open purple diamonds, excitation from E_L=0.445eV to 0.616eV; Δ open red triangles, E_L=0.0.616eV to 0.796eV. For E_0=10eV, ○ orange open circles, CH_2-stretch mode at E_L=0.350 of Dampc *et al*. [6] multiplied by a scaling factor of 1.3. See text for discussion.

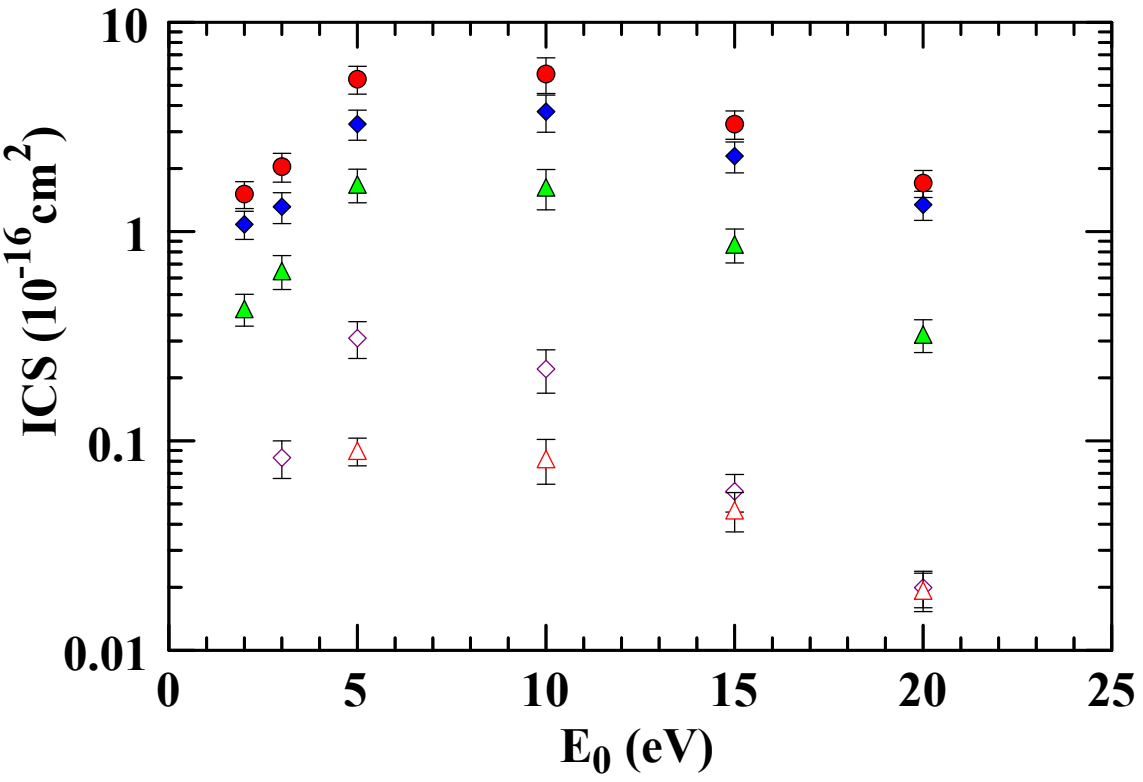

Figure 3 (Color Online): Integral cross-sections for vibrational excitation of THF as a function of E_0. Legend is the same as in Figure 2.